Appl. Phys. B (2017) 123:176
DOI 10.1007/s00340-017-6746-3

Applied Physics B
Lasers and Optics

# $CO_2$ laser polishing of conical shaped optical fiber deflectors

**Elif Uzcengiz Şimşek[1,2] · Bartu Şimşek[1,2] · Bülend Ortaç[1,2]**

Received: 29 October 2016 / Accepted: 13 May 2017 / Published online: 25 May 2017


**Abstract** A novel method for polishing conical shaped optical fiber deflectors by modulated $CO_2$ laser exposure is reported. The conical shaped fiber deflector geometry was first formed with rough mechanical polishing, then it was exposed to modulated $CO_2$ laser operating with wavelength at 10.6 μm to achieve fine polish surfaces. The motivation of this work is to demonstrate that the modulated $CO_2$ laser exposure approach allows a fiber surface roughness at a nanometer scale without modifying the conical shape of the fiber deflector. The average surface roughness of mechanically polished fiber deflectors with 30 and 9 μm lapping films was smoothed down to 20.4 and 4.07 nm, respectively, after $CO_2$ laser polishing process. By combining mechanical and laser polishing techniques, fabrication of conical shaped optical fiber deflectors takes less time and it becomes laborer independent and easy to apply.

## 1 Introduction

Fiber optical probes are ideal tools for numerous applications such as material processing, imaging, and spectroscopy. The use of fiber optical probes for medical treatment opens the door for minimally invasive surgery applications, as they possess a smaller size and efficiently transmit the laser light with different shapes and directions by manipulating their deflector's geometry. Different deflector designs have been proposed and several types are currently used for tissue ablation. The types of deflector shapes are bare, side-firing and radial. Bare fiber optic deflectors (basic deflector geometry) transmit the laser energy in the same direction along the fiber. Side-firing optical fiber optical deflectors transmit laser light perpendicular to the fiber axis through specific direction and they are widely used in many medical applications, especially in the prostate tumor ablation [1]. One of the most popular deflector types is radial design. Radial fiber optic deflectors with conically shaped optical fiber end transmit the laser energy radially and the laser energy is homogeneously distributed into a ring-shaped beam. These deflectors are especially used in endovenous laser ablation (EVLA) [2]. Unlike other cone-shaped fiber optical probes [3–7] used for various applications, EVLA operation needs μm-scale, multimode (MM) optical fibers and specific cone-angle values to fulfill the EVLA operation requirements. Thus, multi-mode, larger NA and μm-scale optical fibers are preferred in the operations. The homogeneous, ring-shaped laser energy distribution can be achieved with large cone angles which are detailed in this study. It allows a perfect irradiation of vein walls and their ablation. Among existent fiber processing methods such as chemical, FIB [3–5], mechanical polishing method is the best candidate to obtain such desired cone-angles. Furthermore, mechanical polishing process is applicable for mass-production of conical shaped optical fibers used in EVLA operation. In the mechanical polishing process, the deflector geometry is first formed with rough lapping film, then, the surface roughness of the deflector is gradually smoothed by polishing with smoother lapping films [8]. This process is composed of several steps to obtain high quality surface structures and a well-prepared fiber deflector surface eliminates the optical losses such as scattering and back reflection. However, the mechanical fining

✉ Bülend Ortaç
ortac@unam.bilkent.edu.tr

[1] Institute of Material Science and Nanotechnology, Bilkent University, 06800 Ankara, Turkey

[2] National Nanotechnology Research Center, Bilkent University, 06800 Ankara, Turkey

process of the fiber deflectors takes very long time and it is laborer dependent. In the paper, we develop a surface treatment technique for polishing conical shaped optical fiber deflectors by combining rough mechanical polishing and nanoscale surface roughness polishing with modulated $CO_2$ laser treatment. In the literature, it was reported that the bare fiber end could be polished down to 100 nm surface roughness by continuous wave $CO_2$ laser exposure [9]. In our approach, the modulated $CO_2$ laser exposure permits the control of thermal loading issue on a thin surface layer and volume melting, surface reflow, deformation of deflector shape could be avoided. A very smooth surface roughness about 4.07 nm can be achieved by using this approach. This also provides less-time consuming and laborer independent procedure. In this paper, the conical fiber deflector requiring meticulous design and fabrication process was investigated in terms of design, surface roughness profile and light deflection measurements.

## 2 Deflection angle calculation and simulation

### 2.1 Ray tracing calculation

Conical shaped fiber deflector provides a side deflection geometry and it forms a circular beam pattern. We used Snell's law and ray tracing calculations for determining the relation between deflection angle and cone angle. Ray tracing method is a powerful tool to identify the light deflection behavior of the conical fiber deflector. The ray tracing pattern of the conical shaped fiber deflector is shown in Fig. 1.

When the laser beam reaches to the deflector, it comes to the first core-air boundary. At this boundary, it is reflected by obeying the total internal reflection (TIR) since the critical angle between core-air boundary, $\theta_{\text{core-air}}$ is calculated as $\theta_{\text{core-air}} = \sin^{-1}(n_{\text{air}}/n_{\text{core}})$ which equals to 43.3° when the deflector angle in the range of $\alpha<\pi-2\theta_{\text{core-air}}$ to obtain side deflection. $\theta_1$ equals to $(180-\alpha)/2$ and $\theta_1$ becomes 60° which means that $\theta_1 > \theta_{\text{core-air}}$ and it confirms the TIR at this boundary. Then, the reflected ray travels through the second core-air boundary and its incoming ray is $\theta_2$ and it is calculated by $\theta_2 = |90 + \theta_1 - \alpha|$ from the geometry. The laser beam is refracted at this boundary; the refraction angle is calculated as $\theta_{\text{refracted}} = \sin^{-1}((n_{\text{core}}/n_{\text{air}})\sin\theta_2)$. Using these calculations, the relation between deflection angles becomes as Eq. 1 [10]:

$$\phi = \frac{180-\alpha}{2} - \theta_{\text{refracted}} \quad (1)$$

Using Eq. 1, $\theta_1$ becomes 60° which means that $\theta_1 > \theta_{\text{core-air}}$ and it confirms the TIR at first core-air boundary, $\theta_2$ becomes 0°, thus, $\theta_{\text{refracted}}$ goes to zero and the deflection angle is found as 60° when the deflector angle is 60° which is in the range of $\alpha<\pi-2\theta_{\text{core-air}}$.

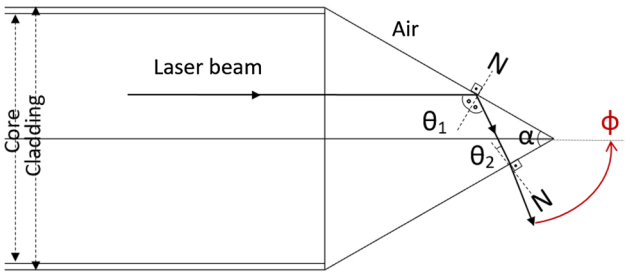


**Fig. 1** Ray tracing paths for the conical shaped fiber deflector

### 2.2 Ray tracing simulation

For further analysis, we also performed numerical simulation analysis. The fiber geometry was created in non-sequential part of Zemax software. We used a fiber having refractive index of core/clad of 1.45/1.39 (Thorlabs, USA) in the air environment. The radius of the core/clad was 600/630 μm and numerical aperture (NA) was 0.39. The rays are coupled inside the fiber (by using fiber.dll source in Zemax) and 10,000 rays were analyzed, only the 50 of the rays are shown in the simulation results (see Fig. 2).

In Fig. 2a, the general overview of simulation configuration is represented. A semi-spherical detector having 50 mm diameter was used to cover the circular beam. The fiber is in the center of the semi-spherical detector. The incoming rays are emitted from the deflector and they form a homogeneous circular beam shape. The 60° deflection angle of the rays is observed and this result is in a good agreement with calculation presented in Eq. 1. In Fig. 2b, the image of the light deflection from conical shaped fiber deflector on semi-spherical detector is represented and a homogeneous circular beam shape could be obtained.

### 2.3 Surface roughness and reflectance relation

In this section, the relation between surface roughness and reflectance is evaluated to estimate the surface roughness level which is necessary to obtain sufficient level of performance. For finding the reflection coefficient at the glass-air boundary, we evaluated our case when the cone-angle is 60°. Since the incoming rays totally reflected from the first surface, they travel at the normal of the second surface which means that the incoming angle is 0°. Thus, in our case, reflection coefficient at the second surface becomes $r_{\text{perp}} \cong r_{\text{par}} = r$. The following equations represent $r_{\text{perp}}$ and $r_{\text{par}}$ in Eqs. 2, 3:

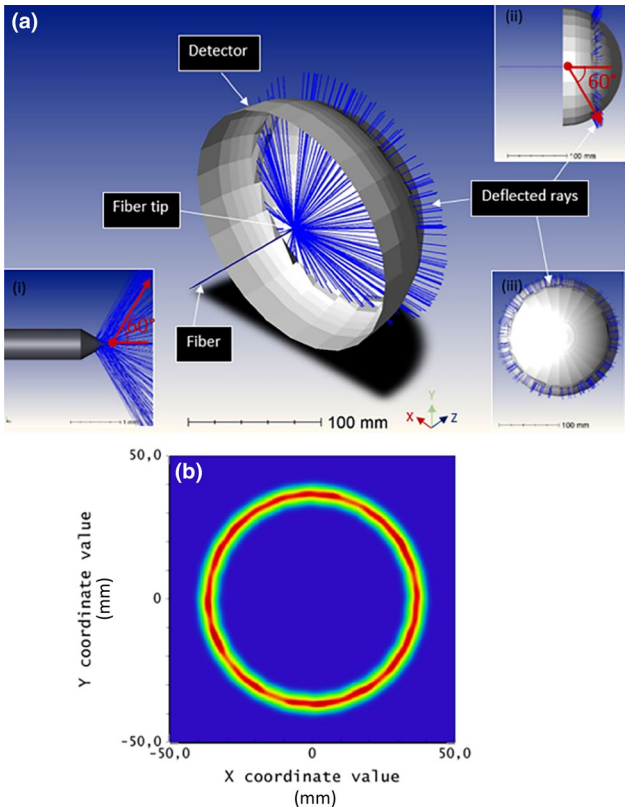


**Fig. 2** Numerical simulation results. **a** Light deflection from the fiber deflector (*i*), Y–Z plane image of the setup (*ii*) and X–Z plane image of the setup (*iii*) and **b** the image of the light deflection from conical shaped fiber deflector on semi-spherical detector

$$r_{\text{perp}} = \frac{n_i \cos\theta_i - n_t \cos\theta_t}{n_i \cos\theta_i + n_t \cos\theta_t}, \tag{2}$$

$$r_{\text{par}} = \frac{n_t \cos\theta_i - n_i \cos\theta_t}{n_i \cos\theta_i + n_t \cos\theta_t}. \tag{3}$$

When the angle between incoming rays and the surface normal is 0°, the equations become as Eq. 4:

$$r = \frac{n_i - n_t}{n_i + n_t} \tag{4}$$

When $n_i = 1.45$ and $n_t = n_{\text{air}} \cong 1$, the reflection coefficient at the second surface boundary is calculated as 0.18. The reflectance, $R$ equals to $r^2$ which is 0.03. Then, using $T = 1-R$, transmission ($T$) at the boundary becomes 0.97. The relation between surface roughness and reflectance is also studied in terms of theory and simulation. The reflectance from a surface depends on $R_s$, the light specularly reflected from the surface and $R_o$, the total amount of light reflected by the sample. The ratio between $R_s$ and $R_o$ is related with the surface roughness value ($\sigma$) and wavelength of the incoming rays ($\lambda$). If the distribution of heights of the surface irregularities is gaussian, this ratio gives rms surface roughness, $\sigma$ in Eq. 5 [8]:

$$\frac{R_s}{R_o} = \exp\left[-\left(\frac{4\pi\sigma}{\lambda}\right)^2\right] \tag{5}$$

When $\sigma$ approaches to $\lambda$, the scattering becomes significant and the ratio between $R_s$ and $R_o$ becomes smaller. To obtain high $R_s$ and $R_o$ ratio, for example 0.9–1, the $\sigma/\lambda$ must be in the range of 0–0.1. In our case, $\lambda$ was 635 nm, thus, surface roughness ($\sigma$) of the cone-shaped deflector must be less than 60 nm to achieve high $R_s/R_o$. Zemax simulations are run to verify the theoretical study. It uses *K*-correlation function to simulate the effect of surface roughness [11]. This function adds roughness to surface of mirrors, lens, optical fibers etc. To evaluate the effect of the surface roughness from the conical shaped deflector, different roughness values were assigned to the end-face of it where the deflection of light occurs. In Fig. 3a, Zemax simulation

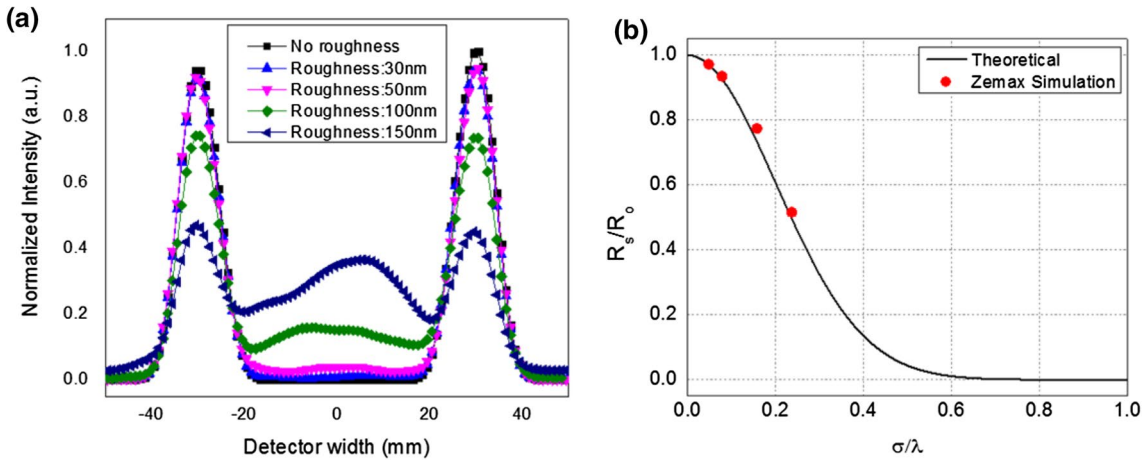


**Fig. 3** **a** The intensity distribution of cone-shaped deflector for different surface roughness values, **b** comparison of the theoretical calculation and Zemax simulation results

was performed for surface roughness values of 30, 50, 100 and 150 nm and the intensity distribution of cone-shaped deflector for different surface roughness values are represented. $R_o$ is considered for the no roughness case, and the other results peak points are taken as $R_s$, $R_s/R_o$ is obtained for each case. In Fig. 3b, comparison of Zemax simulation and the theoretical results are shown. The theoretical function and the simulation results have a good agreement.

## 3 Material and method

### 3.1 $CO_2$ laser–silica interaction

Silica ($SiO_2$) is the main ingredient of most glasses and has a tetrahedral structure with one silicon (Si) bound to four oxygen atoms. Silica has a wide range of high optical transparency from ultraviolet (UV) region of 0.2 μm to infrared (IR) spectral region of 3.5 μm. Light absorption of glass in the range below 0.3 μm is dominated by electronic excitation of molecules, while molecular vibrations are dominated in the IR range [12]. In IR regime, the band of high absorption in the wavelength range of 8 to 11 μm is attributed to the bond-stretching vibration between the Si and O atoms in a Si–O–Si bridge structure. On the other hand, $CO_2$ laser operating in IR regime is a potential laser candidate and it is relatively cheaper than sources operating in UV regime. $CO_2$ lasers are also easy to access and effective sources to processing silica glass. The central wavelength of $CO_2$ laser is around 10.6 μm and photon energy is approximately 0.2 eV. The radiation of $CO_2$ laser is not enough to brake the bonds of Si–O, so it is strongly absorbed by Si–O vibrational modes and converted into heat. Depending on $CO_2$ laser parameters, particularly pulse duration, pulse repetition frequency, peak power, and spot diameter, $CO_2$ laser could be used for polishing of silica glass. In the laser polishing process, high repetition rate laser pulses with relatively low axial irradiance generate a raised temperature on the glass surface, sufficient to melt a thin surface layer that flows under surface tension. For fused silica, generation of a highly mobile glass layer is obtained without significant mass loss when the glass viscosity is in the range between $10^2$ and $10^5$ Pa s. This range corresponds to surface temperatures from 2000 to 2700 °C [13]. In the literature, there are reports on glass processing by controlling the glass viscosity below the ablation threshold using a $CO_2$ laser beam. These works provide an improvement of the surface damage resistance in fused silica optics [14, 15], localized repairing of damages in fused silica optics [16–18], laser polishing of conventional glasses [19, 20] and optical fiber end surfaces [9, 21] and, also, in the manufacturing of micro-optical components. In our approach, modulation of $CO_2$ laser takes an important place for smoothing the silica glass and fiber surfaces without deforming the delicate conical shaped optical fiber deflectors. Below the silica ablation threshold, the heat penetration depth (1D) is smaller than the laser spot diameter and the surface temperature is kept down by the pulse energy for short pulse widths. For longer pulses; on the contrary, the penetration depth is increased along both radial and axial direction with larger heated spot radius [22]. When the pulsed $CO_2$ laser exposed on $SiO_2$ surface, the energy dissipated in several μm depth and the surface of glass melts and gets into fluidic phase and it turns into solid when the exposure is over. The cracks and scratches located on the silica glass or optical fiber surface are eliminated and smoothened under favor of this process. On the other hand, applying longer pulses or continuous wave $CO_2$ laser to process silica glass or optical fiber causes deformation on its structure, such as forming ball lens at the end of optical fiber.

## 4 Experimental section

### 4.1 Sample preparation and $CO_2$ laser treatment process

The cone-shape was first formed by one step rough mechanical polishing process using mechanical polishing machine (Ultrapol, USA). There are two types of mechanical polished fibers which are prepared with 30 and 9 μm lapping films. The deflector angle of both fibers was adjusted as ~60°. The traditional mechanical polishing procedure continues with finer lapping films in order to decrease the roughness of the fiber deflector. Instead of continuing with mechanical fine polishing, the cone-shaped fiber deflectors could be smoothened by one step $CO_2$ laser exposure procedure. The $CO_2$ laser exposure was modulated since continuous-wave laser exposure may change the shape of the fiber deflector. The cone-shaped fiber deflector is prone to be a ball lens after being exposed to continuous-wave $CO_2$ laser, thus, a special function was developed to modulate the laser. The fiber glass processing machine LZM 100 (AFL, Japan–USA) for controlled $CO_2$ laser polishing experiment is illustrated in Fig. 4a. The fiber is homogeneously exposed to the laser from both sides of the fiber deflector. The shutter was used to modulate the laser beam. The fiber processing machine could show the hot images of the fiber during the process. Hot images are visual data guiding the process to give the information on the evolution of deflector geometry during the laser exposure. The graph shown in Fig. 4b was plotted by the machine itself based on the laser average power data vs. time data taken by thermo-coupled detector. We have performed several configurations (laser power, pulse

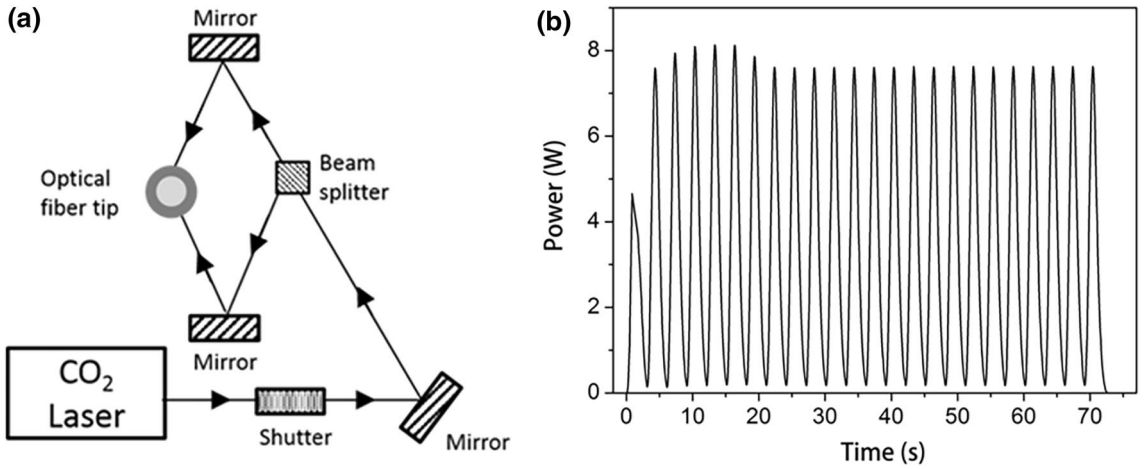


**Fig. 4** **a** $CO_2$ laser processing setup, **b** modulated $CO_2$ laser output power vs. time graph

duration, number, and period) in order to optimize the laser polishing process. In the machine settings, there is a function to determine laser power which is the minimum power to melt standard single mode fiber (SMF). Editing this function, we designated the minimum laser power to melt our fibers using in the experiment. The selected power intensity of the beam was $9.15 \times 10^3$ W/cm$^2$. After selecting laser power, we have performed different laser pulse durations (0.75, 1 and 1.25 s) on conical shaped optical fibers. 0.75 s laser pulse was not enough to melt fiber surface, so we investigated the effect of 1 s and 1.25 s pulses on fiber surface and shape. The laser pulse of 1.25 s transform the shape of fiber deflector into ball shaped fiber end. Therefore, the pulse duration of $CO_2$ laser was determined as 1 s.

Number and period of laser pulse are also important steps of optimization process. Period of pulse was determined by investigating thermal behavior of heated fiber tip. The $CO_2$ laser was modulated as 1-s duration and 2-s interval to cool surface of fiber efficiently. In order to get minimum number of pulse, we have designed the study for 30 and 9 μm polished fibers. We have applied three different numbers of pulse values; 8, 16 and 24 pulses for each fiber tip polished at both 30 and 9 μm lapping films. We obtained SEM images of each fiber surface as seen in the Table 1. When we analyze the results, 8 laser pulse is clearly insufficient, 16 laser pulse gives smooth surface and 24 pulse gives best results in terms of surface roughness of conical shaped optical fiber deflectors. As a result of optimization process, the geometry of the $CO_2$ laser-polished fiber deflector remained as cone-shaped, and the fiber end-face surface is gradually smoothed by laser exposure.

## 5 Results and discussion

In Fig. 5a, SEM image of the fiber deflector polished with commercially available 30 μm lapping film (Krell Tech, USA) is shown. The rough fiber surface was exposed to modulated $CO_2$ laser beam. A smooth fiber deflector surface was successfully obtained as shown in Fig. 5b, after $CO_2$ laser surface treatment. Due to the larger initial surface roughness structures obtained by mechanical polishing process, we also observed surface waviness. In the second experiment, we used 9 μm lapping film for rough mechanical polishing. The conical shaped fiber optical deflector geometry is obtained. In Fig. 5c, SEM image of the fiber deflector polished with 9 μm lapping film (Krell Tech, USA) is shown. We also applied the same $CO_2$ laser treatment procedure. The conical shape of the deflector is protected after laser exposure and the SEM image of the deflector (see Fig. 5d) demonstrated that the surface quality of the deflector is definitely improved.

In order to study the surface morphology of the deflectors, the AFM analysis was performed. AFM surface roughness images are represented in Fig. 6. The mechanically polished fiber end-face surfaces could not be analyzed since their surfaces were much rough for the AFM deflector. Any clear image of the fiber deflectors polished with 30- and 9 μm-rough lapping films could not be obtained to avoid damaging the AFM tip. After the $CO_2$ laser exposure, the fiber surfaces were smoothened, and we were able to study the surface profiles by AFM. $4 \times 4$ μm area was scanned by the AFM deflector. The conical surface of the fiber deflector restricted the area that we could scan since it has a curved surface. The average surface roughness of mechanically polished fiber

**Table 1** SEM images of conical shaped optical fiber deflectors with different number of pulses and initial lapping film

| # of pulses / Lapping film | 8 | 16 | 24 |
|---|---|---|---|
| 30µm | 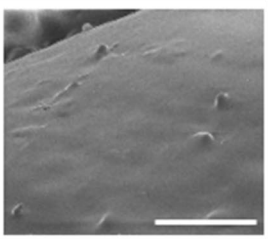 | 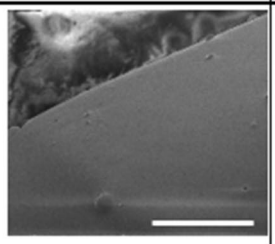 | 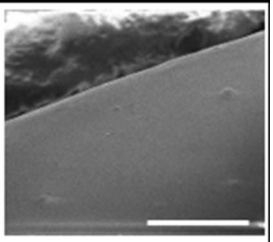 |
| 9µm | 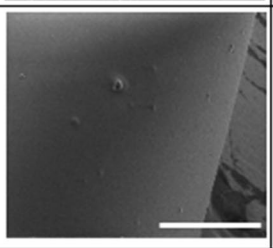 | 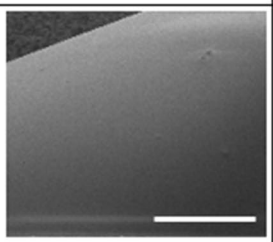 | 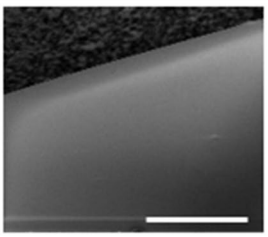 |

*Scale bars* 50 µm

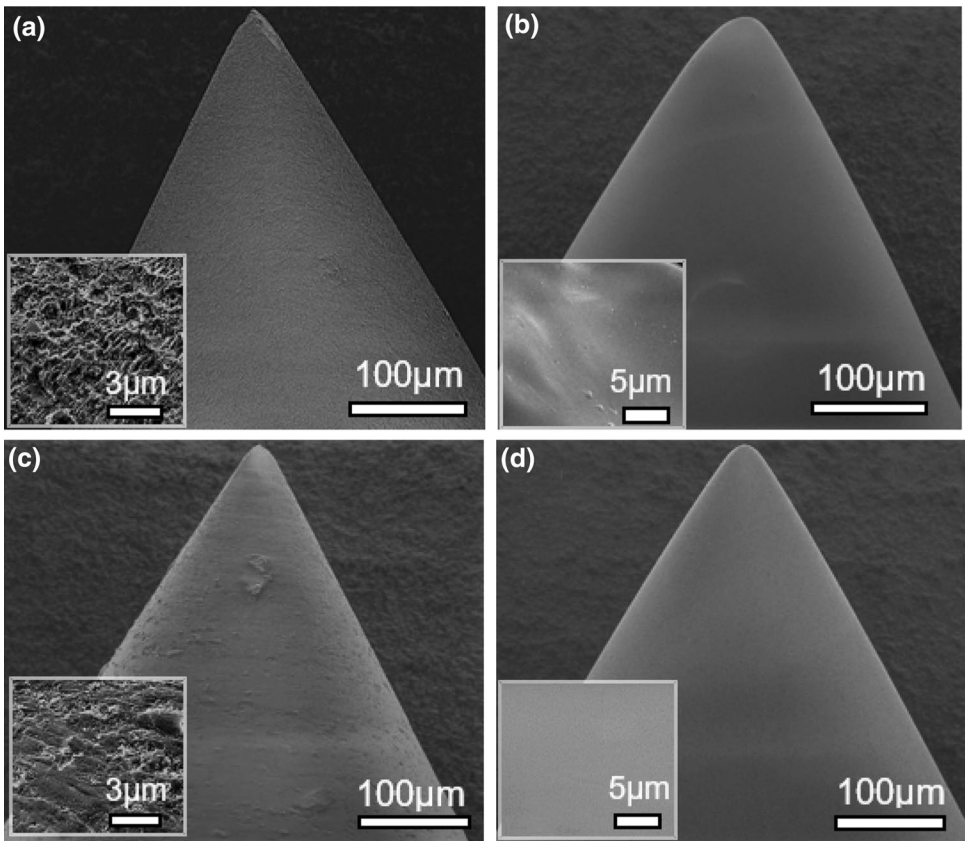


**Fig. 5** SEM images of fiber deflectors **a** polished on 30 µm-rough film, **b** after exposure to modulated $CO_2$ laser and **c** polished on 9 µm-rough film, **d** after exposure to modulated $CO_2$ laser (*insets* show the zoomed area)

deflectors with 30 and 9 µm lapping films were smoothed down to 20.4 and 4.07 nm, respectively, after $CO_2$ laser polishing process.

Our approach clearly demonstrates that sub-10 nm average surface roughness of conical shaped fiber deflectors could be obtained by combining rough mechanical and

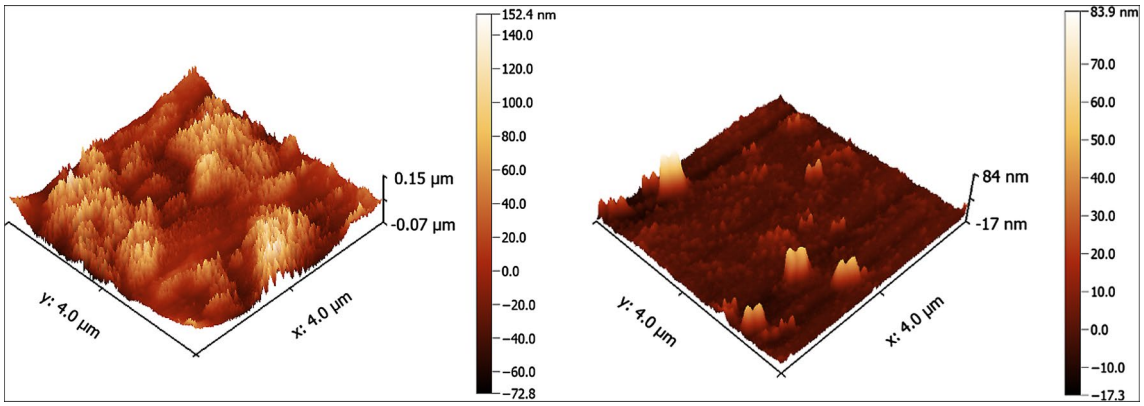


**Fig. 6** AFM images of fiber deflectors **a** mechanically polished with 30 µm lapping film and modulated $CO_2$ treatment, **b** mechanically polished with 9 µm lapping film and modulated $CO_2$ treatment

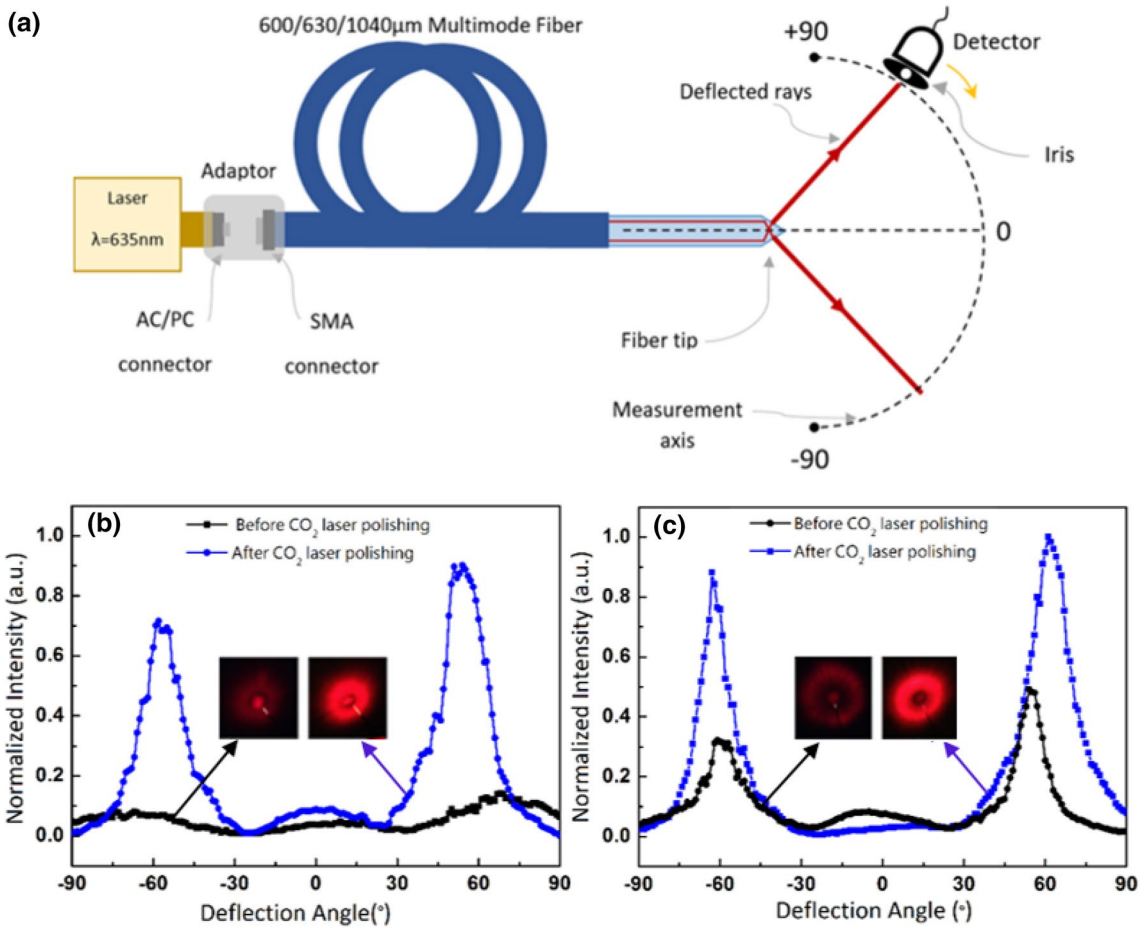


**Fig. 7** **a** Characterization of spatial light distribution of the conical shaped fiber deflectors. Spatial light distribution graphs of fiber deflectors mechanically polished with 30 µm lapping film (*black line*) and modulated $CO_2$ treatment (*blue line*) **b** and mechanically polished with 9 µm lapping film (*black line*) and modulated $CO_2$ treatment (*blue line*) **c** and the insets in the graphs belong to the demonstration of circular light deflection from conical shaped deflectors for each measurement

fine $CO_2$ laser polishing process. The surface roughness of the fiber deflector affects the light deflection properties. In order to analyze the effect of the surface roughness to the light deflection, the spatial light distribution of the fiber deflectors was measured by the home-built characterization setup represented in Fig. 7a. The detector located on the rotating stage revolves around the optical fiber deflector while collecting the power data. An aperture was attached in front of the detector to analyze light deflection more accurately. A fiber coupled diode laser emitting at 635 nm (ThorLabs, USA) was launched to the optical fiber. Light deflection was measured on mechanically polished deflector and $CO_2$ laser polishing treated deflector. The normalized intensity vs. deflection angle graph of the fiber deflectors was plotted according to data obtained from the setup in Fig. 7a. In Fig. 7b, c, black line belongs to light deflection of the fiber deflector which was mechanically polished with 30 and 9 µm lapping films.

The intensity distribution does not change significantly along the plot. This means that mechanically polished deflector scatters all coming light. After applying the $CO_2$ laser polishing to mechanically polished deflector, the intensity of the $CO_2$ laser-treated fiber deflector increased 8.6 times comparing to the intensity of non-treated deflector. The blue line represents the light intensity distribution after laser polishing. The center of maximum light intensity of the laser polished deflector is 58° deflection angle. In Fig. 7c, black line belongs to deflection of the fiber deflector mechanically polished with 9 µm-lapping film. The blue line shows the light intensity after the $CO_2$ laser polishing of the deflector. The intensity of the $CO_2$ laser-treated fiber deflector was 2.8 times more than the intensity of non-treated deflector. The insets in Fig. 7b, c demonstrate light deflection from untreated and treated fiber surfaces and the deflected power. Light distribution increased due to elimination of the cracks and scratches by the $CO_2$ laser exposure. In this case, the center of maximum light intensity of the laser-polished deflector is 62° deflection angle. The deflection angle of both cases was in agreement with the calculated values of our design (Eq. 1). The FWHM of light deflection beam outputs for both before and after $CO_2$ laser exposure were measured. For the case in Fig. 7b, the FWHM of the beam output of mechanically polished fiber deflector was decreased from 49° to 18.7°, and for Fig. 7c the FWHM decreased from 20° to 13° after $CO_2$ treatment of fiber deflector surface. This also indicates the surface smoothening of fiber deflector by $CO_2$ laser exposure for both experiments.

## 6 Conclusion

The conical shaped optical fiber deflectors have been developed through a two-step polishing techniques of combining mechanical and $CO_2$ laser treatments. Once the conical shape of the fiber deflectors is formed by 30 µm- and 9 µm-rough polishing films, a modulated $CO_2$ laser process is applied to obtain very smooth fiber deflector surface. The rest of the mechanical polishing procedure could be omitted due to easy and fast $CO_2$ laser polishing. AFM surface analysis shows that the roughness of the mechanically polished fiber deflectors at 30 and 9 µm films can be decreased down to 20.4 and 4.07 nm, respectively, after optimized $CO_2$ laser polishing. A new method of combining mechanical and $CO_2$ laser polishing makes the fabrication of conical fiber deflectors easy, fast and laborer independent.

**Acknowledgements** We thank Mustafa Fadlelmula for his assistance with atomic force spectroscopy (AFM) analysis. We would also like to show our gratitude to Canan Kurşungöz for reading and making comments that improved the manuscript.

## References

1. A.K. Ngo, N.M. Fried, Side-firing germanium oxide optical fibers for use with erbium: YAG laser. J. Endourol. **20**(7), 475–478 (2006)
2. F. Pannier, E. Rabe, J. Rits, A. Kadiss, U. Maurins, Endovenous laser ablation of great saphenous veins using a 1470 nm diode laser and the radial fibre–follow-up after six months. Phlebology **26**(1), 35–39 (2011)
3. A. Kuchmizhak, S. Gurbatov, A. Nepomniaschii, O. Vitrik, Yu. Kulchin, High-quality fiber microaxicons fabricated by a modified chemical etching method for laser focusing and generation of Bessel-like beams. Appl. Opt. **53**, 937–943 (2014)
4. Raoul Stöckle, Christian Fokas, Volker Deckert, Renato Zenobi, High-quality near-field optical probes by tube etching. Appl. Phys. Lett. **75**, 160 (1999)
5. S. Cabrini, C. Liberale, D. Cojoc, A. Carpentiero, M. Prasciolu, S. Mora, V. Degiorgio, F. De Angelis, E. Di Fabrizio, Axicon lens on optical fiber forming optical tweezers made by focused ion beam milling. Microelectron. Eng. **83**, 804–807 (2006)
6. T. Grosjean, S.S. Saleh, M.A. Suarez, I.A. Ibrahim, V. Piquerey, D. Charraut, P. Sandoz, Fiber microaxicons fabricated by a polishing technique for the generation of Bessel-like beams. Appl. Opt. **46**, 8061–8067 (2007)
7. S.-K. Eah, W. Jhe, Nearly diffraction-limited focusing of a fiber axicon microlens. Rev. Sci. Instr. **74**, 4969 (2003)
8. J.M. Bennett, R.J. King, Effect of polishing technique on the roughness and residual surface film on fused quartz optical flats. Appl. Opt. **9**, 236–238 (1970)
9. U. Mircea, H. Orun, A. Alacakir, Laser polishing of optical fiber end surface. Opt. Eng. **40**(9), 2026–2030 (2001)
10. T. Watanabe, Y. Matsuura, Side-firing sealing caps for hollow optical fibers. Lasers Surg. Med. **38**(8), 792–797 (2006)
11. S. Gangadhara, "How to model surface scattering via the K-correlation distribution", published on 2008, updated on 2010. www.zemax.com. Received on 21 Jan 2017
12. D.W. Lane, The optical properties and laser irradiation of some common glasses. J. Phys. D Appl. Phys. **23**(12), 1727 (1990)
13. K.L. Wlodarczyk, Surface deformation mechanisms in laser smoothing and micromachining of optical glasses, Diss. Heriot-Watt University, 2011

14. P.A. Temple, W.H. Lowdermilk, D. Milam, Carbon dioxide laser polishing of fused silica surfaces for increased laser-damage resistance at 1064 nm. Appl. Opt. **21**(18), 3249–3255 (1982)
15. P. Cormont, P. Combis, L. Gallais, C. Hecquet, L. Lamaignère, J.L. Rullier, Removal of scratches on fused silica optics by using a $CO_2$ laser. Opt. Express **21**, 28272–28289 (2013)
16. N. Shen, M.J. Matthews, J.E. Fair, J.A. Britten, H.T. Nguyen, D. Cooke, S. Elhadj, S.T. Yang, Laser smoothing of sub-micron grooves in hydroxyl-rich fused silica. Appl. Surf. Sci. **256**(12), 4031–4037 (2010)
17. C. Buerhop, B. Blumenthal, R. Weissmann, Glass surface treatment with excimer and $CO_2$ lasers. Appl. Surf. Sci. **46**(1-4), 430–434 (1990)
18. S. Palmiera, L. Gallaisa, M. Commandréa, P. Cormontb, R. Courchinouxb, L. Lamaignèreb, J.L. Rullierb, P. Legrosc, Optimization of a laser mitigation process in damaged fused silica. Appl. Surf. Sci. **255**(10), 5532–5536 (2009)
19. M. Serhatlioglu, B. Ortaç, C. Elbuken, N. Biyikli, M. Solmaz, $CO_2$ laser polishing of microfluidic channels fabricated by femtosecond laser assisted carving. J. Micromech. Microeng. **26**, 115011 (2016)
20. F. Laguarta, N. Lupon, J. Armengol, Optical glass polishing by controlled laser surface-heat treatment. Appl. Opt. **33**(27), 6508–6513 (1994)
21. A. Kuhn, P. French, D.P. Hand, I.J. Blewett, M. Richmond, J.D. Jones, Preparation of fiber optics for the delivery of high-energy high-beam-quality Nd: YAG laser pulses. Appl. Opt. **39**(33), 6136–6143 (2000)
22. E. Mendez, K.M. Nowak, H.J. Baker, F.J. Villarreal, D.R. Hall, Localized $CO_2$ laser damage repair of fused silica optics. Appl. Opt. **45**(21), 5358–5367 (2006)